Pergamon

Int. J. Multiphase Flow Vol. 22, No. 2, pp. 223–238, 1996

0301-9322(95)00067-4
0301-9322/96 $15.00 + 0.00

PERFORMANCE OF AN AIR-LIFT PUMP FOR CONVEYING COARSE PARTICLES

T. YOSHINAGA[1] and Y. SATO[2]

[1]Nishinippon Institute of Technology, Kanda-cho, Miyakogun, Fukuoka 800-03, Japan

[2]Department of Mechanical Engineering, Kumamoto University, Kumamoto 860, Japan

(Received 10 April 1995; in revised form 6 September 1995)

Abstract—Experiments were made with either uniform spherical particles or non-uniform spherical particles using air and water as the working fluids. In the experiments, the diameter of the upriser, the diameters of the particles and the submergence ratio were changed systematically. The obtained data showed that the operation performance of an air-lift pump can be clearly characterized by the triangular relationship between the flow rates of the water and particles discharged and the flow rate of the air supplied. A model which describes the flows in the upriser is proposed based on a momentum equation. The experimental and predicted characteristics of the flow are shown to be in good agreement.

Key Words: air-lift pump, coarse particles, three-phase flow, two-phase flow

1. INTRODUCTION

An air-lift pump has been used as a means of lifting corrosive and/or toxic liquids in chemical industries, and of conveying slurries in mining. More recently, it has been recognized that an air-lift pump has the potential to convey manganese nodules from deep seabeds, e.g. Giot (1982). To establish the design method for such a system, it is important to obtain adequate models predicting flows in the system, i.e. two-phase water–coarse particle flow and three-phase air–water–coarse particle flow. For this, there is also a need to provide designers with appropriate data on the operation performance of an air-lift pump conveying coarse particles.

Experimental studies so far made in this area are those of Kawashima *et al.* (1975), Weber & Dedegil (1976) and Usami & Saito (1986). They performed experiments using uniform particles. Kawashima *et al.* (1975) has examined the relationship between the volumetric fluxes of air supplied and particles discharged, changing the volumetric concentration of the particles. In their experiment, the particles used were small (about 1.7 mm in diameter), the submergence ratio was 0.92 and the volumetric flux of air was low, lower than 3 m/s. Weber & Dedegil (1976) have performed an experiment with a large and tall air-lift pump which conveyed gravel. Although their data are especially valuable, the upriser length, suction height, volumetric concentration of the particles discharged and the submergence ratio were different from run to run. Usami & Saito (1986) have performed an experiment on an air-lift pump which conveyed simulated manganese nodules. In their experiment, the submergence ratio was 0.82. Since the experimental results of the above three experiments are not always systematic, it is difficult to clearly understand from such results the operation performance of an air-lift pump.

Theoretical studies have been made for uniform particles by Kato *et al.* (1975), Kawashima *et al.* (1975), Giot (1982), Usami & Saito (1986), Dedegil (1987) and Tomiyama *et al.* (1992). These studies are based on momentum balance (Kato *et al.*, Giot and Usami & Saito), empirical correlations (Kawashima *et al.*), power balance (Dedegil) and a multi-fluid model (Tomiyama *et al.*). Although the momentum balance method is principally a sound approach, the respective authors have not confirmed the validity of their proposed method with experimental data other than the relating authors'. Similarly, the above-mentioned empirical correlations and power balance method have not been confirmed by experimental data other than the relating authors'. The multi-fluid model is not satisfactorily applicable yet because several constitutive equations for three-phase flow are insufficient as mentioned in the report. As a result, none of models, together with their relating constitutive equations, have been sufficiently successful yet to be used in engineering.

To provide an additional data base on an air-lift pump conveying coarse particles, we performed experiments using either uniform coarse particles or non-uniform coarse particles. In the experiments, the diameter of the upriser, the size of the particles and the submergence ratio were changed systematically. In this report, we present the results by showing the triangular relationship between the flow rate of the air supplied and the flow rates of the water and particles discharged. Secondly, we propose a method for predicting the operation performance based on a momentum equation. To examine the validity of the method, we compare the predicted results with the experiments performed by the above-mentioned investigators as well as with the present experiments.

2. EXPERIMENTS

Operation performance of an air-lift pump which conveys particles can be characterized by the triangular relationship between the flow rates of the water and particles discharged and the flow rate of air supplied. To see such an operation performance, we performed experiments using ceramic spheres as the particles, and air and water as the working fluids. In the experiments, the diameter of the spherical particles, the diameter of the upriser and the submergence ratio were systematically changed.

2.1. Experimental apparatus and procedure

The experimental apparatus used is schematically shown in figure 1. The body of the air-lift pump was a vertical pipe consisting of an upriser, L_1, and a suction pipe, L_2. A suction box, into which the suction pipe was inserted, was connected to a water reservoir by means of a large aqueduct. The amount of water in the water reservoir was controlled by regulating the level of an overflow tank. A pumping action was caused by injecting air into the upriser through an air injector. Test particles, which fell down through the pipe by gravity from the particle feeders to the suction box, were sucked into the suction pipe along with the water. The air-lift pump was steadily operated by supplying air and particles at each fixed flow rate and by keeping the water level in the water reservoir constant. The flow rate of the air supplied was adjusted with a range of error within $\pm 3\%$. At the air injector, the air flow was merged into the two-phase water–solid mixture flowing into the suction pipe. The three-phase air–water–solid mixture then flowed upward in the upriser, and was discharged into an air separator. The air was freed into the atmosphere, and the water–solid mixture flowed down to a particle–water separator. To measure the respective flow rates of the

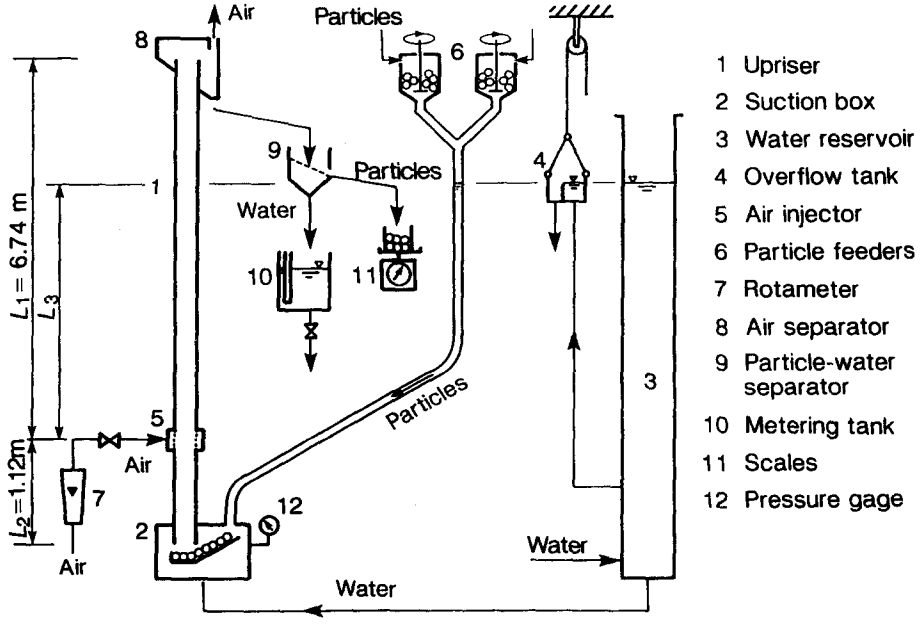

Figure 1. Experimental apparatus.

Table 1. Details of test particles

Symbol	Material	Density ρ_S(kg/m^3)	Shape	Diameter d_S(mm)	Free falling velocity u_{ST}(m/s)	Particle Reynolds number Re_S
C1-Sp-06	ceramics	2540	sphere	6.1	0.541	3280
C1-Sp-10	ceramics	2540	sphere	9.9	0.689	6760
C2-Sp-06	ceramics	3630	sphere	6.0	0.701	4160
C2-Sp-10	ceramics	3630	sphere	9.5	0.885	8390

water and the particles, the water was led to a metering tank while the particles were led to scales. The respective flow rates of the water and the particles were measured 5–10 times to determine the average for every run. The scatter bands of those experimental values were within about 3%, respectively.

Two air-lift pumps were prepared in order to examine the influence of pipe diameter on the operation performance. One was 40 mm and the other was 26 mm in diameter. Each was an upriser ($L_1 = 6.74$ m) connected with a suction pipe ($L_2 = 1.12$ m) as shown in figure 1. The inside surfaces of these pipes were smooth.

Uniform particles and non-uniform particles were used in the present experiments. (Details of the particles will be presented in section 2.2.) The non-uniform particles were made up of two kinds, 6 and 10 mm in diameter. As shown in figure 1, two particle feeders were perpared to supply non-uniform particles at respective fixed flow rates. The flow rate of each particle was set with a suitable orifice mounted at the center of the bottom of each feeder. To keep this flow rate constant, the particles were stirred with a rotating blade. At the weighing point, the particles discharged were classified using a riffler and the flow rates of the particles were measured for each size.

The submergence ratio, which is defined as $\alpha = L_3/L_1$, was controlled by regulating the submergence height, L_3. The submergence height, which was approximately equal to the water level in the water reservoir, was accurately measured using a pressure gauge installed at the same level as the inlet of a suction pipe. The submergence ratio was controlled to a scatter band within $\pm 0.3\%$.

2.2. *Test particles*

The particles used were ceramic spheres, the characteristics of which are listed in table 1. Each symbol given to the particles is denoted by its material, shape and diameter. For example, C1-Sp-06 stands for ceramic with a density of $\rho_S = 2540$ kg/m^3, sphere in shape and 6 mm in diameter. The free terminal velocity, u_{ST}, and the particle Reynolds number, $Re_S = u_{ST} d_S / \nu_L$, are shown in this table. The drag coefficient, C_D, was about 0.42 for the respective particles.

2.3. *Experimental conditions*

Experiments were performed using air and water at atmospheric temperature and pressure. The particles used were of two types: uniform particles and non-uniform particles (which were made up of two kinds).

Conditions for the experiments with uniform particles are listed in table 2. The submergence ratios, α, were 0.6, 0.7 and 0.8. The volumetric flux of air, j_G, reduced at 20°C and the atmospheric pressure was varied from 0.1 to 12.3 m/s. Three kinds of uniform particles, C1-Sp-06, C1-Sp-10 and C2-Sp-06, shown in table 1, were prepared as test particles. The volumetric flux of the particles, defined as $j_S = Q_S/A$, was varied form 0 to 0.14 m/s, where Q_S and A are the volumetric flow rate of the particles and the cross-sectional area of the pipe, respectively. The volumetric concentration

Table 2. Conditions for the experiments with uniform particles

Pipe diameter, D(mm)	40 and 26
Pipe length	
upriser length, L_1(m)	6.74
suction height, L_2(m)	1.12
Submergence ratio, α	0.8, 0.7 and 0.6
Volumetric flux of air, j_G(m/s)	max. 12.3
Volumetric flux of particles, j_S(m/s)	max. 0.14

Table 3. Conditions for the experiments with non-uniform particles which were different in size

Pipe diameter, D(mm)	40
Pipe length	
upriser length, L_1(m)	6.74
suction height, L_2(m)	1.12
Submergence ratio, α	0.8
Volumetric flux of air, j_G(m/s)	max. 8.4
Particles	
mass flow rate, M_S(kg/s)	0.10, 0.20 and 0.30
combination	C1-Sp-06 and C1-Sp-10 and C1-Sp-06 and C2-Sp-10
mixing ratio, M_S^*	0, 1/3, 2/3 and 1

of particles discharged, defined as $\beta_S = j_S/(j_L + j_S)$, was varied from 0 to 0.185, where j_L is the volumetric flux of water discharged.

Conditions for the experiments with non-uniform particles are listed in table 3. In these experiments, the pipe diameter of the air-lift pump, D, was 40 mm; the submergence ratio was set at 0.8; j_G was varied up to 8.4 m/s; and the mass flow rates of the particles, M_S, were 0.10, 0.20 and 0.30 kg/s. The test particles consisted of two cases: a combination of C1-Sp-06 and C1-Sp-10 and a combination of C1-Sp-06 and C2-Sp-10. The former was made up of two kinds of particles different in size but of the same density, and the latter was made up of two kinds of particles different in both size and density. The mixing ratio, M_S^*, defined in the following equation, was set constant in each run:

$$M_S^* = \frac{M_{S1}}{M_S}, \qquad [1]$$

where M_{S1} is the mass flow rate of C1-Sp-06. In reality, M_S^* was set constant at each of the following four stages; 0, 1/3, 2/3 and 1.

3. EXPERIMENTAL RESULTS

3.1. Operation performance of an air-lift pump

An example of the experimental results of an air-lift pump is shown in figure 2 in terms of the volumetric fluxes of the three phases, j_G, j_L and j_S. The experimental data have been obtained from

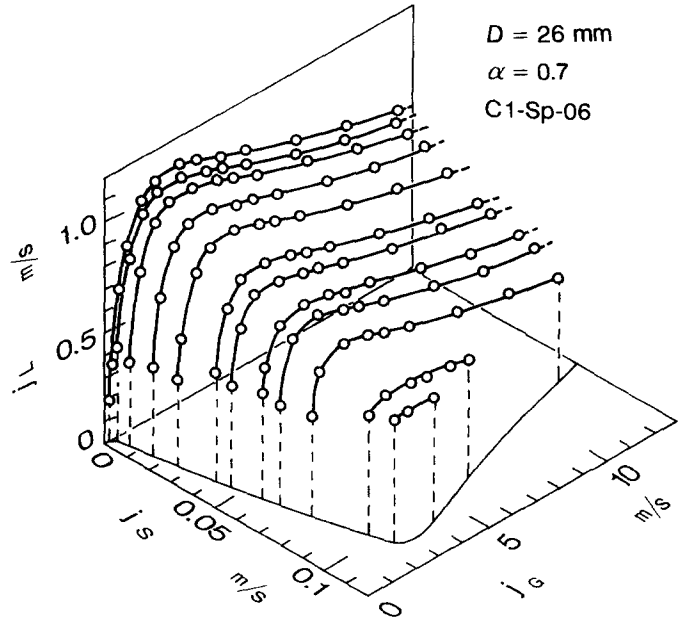

Figure 2. Triangular relationship between the volumetric flux of air supplied, and the volumetric fluxes of water and particles discharged.

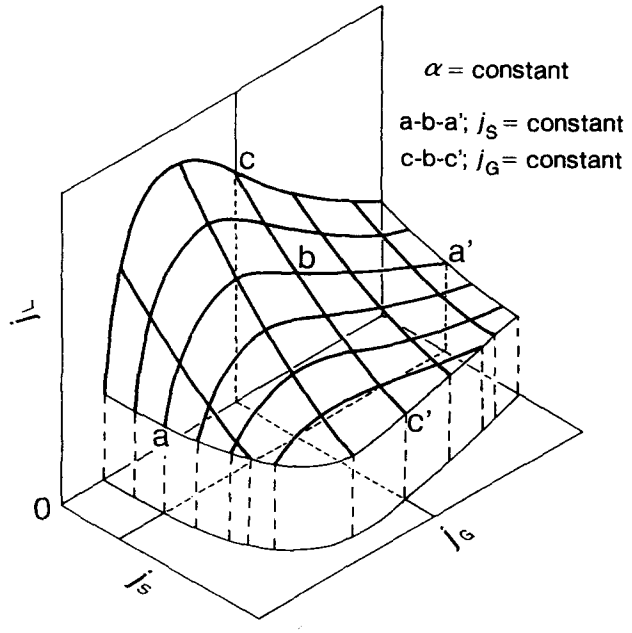

Figure 3. Explanatory diagram of the operation performance of an air-lift pump.

the upriser of 26 mm in diameter, at the submergence ratio of 0.7 and with uniform spherical particles of $d_S = 6.1$ mm and $\rho_S = 2540$ kg/m^3. Bold lines in figure 2 show the relationships between j_G and j_L at a constant j_S. The line at $j_S = 0$ is a well-known operation curve of an air-lift pump which lifts water only. Each curve at a constant j_S is similar to the tendency at $j_S = 0$ and has the following feature: with increasing j_S, the range of j_G where the particles can be conveyed becomes narrow, and j_L becomes low. A fine curve on the j_G–j_S plane represents the boundary where the particles can be conveyed.

From the observation in figure 2, an explanatory diagram of the operation performance of an air-lift pump when it conveys particles is drawn in figure 3. The curved surface represented by the bold lines shows the relationship between j_G, j_L and j_S. The steady state operation of such an air-lift pump can be characterized by a point on this curved surface. The curve a–b–a′ represents an operation curve of an air-lift pump when j_S is constant. An air-lift pump operates, in general, at a constant j_G. In such a case the operation curve becomes like the curve c–b–c′.

3.2. Influence of size, density and flow rate of the particles on operation performance

Figure 4(a)–(c) shows the experimental results of an air-lift pump when it conveys non-uniform spherical particles at three mass flow rates, $M_S = 0.10$, 0.20 and 0.30 kg/s. The particles were made

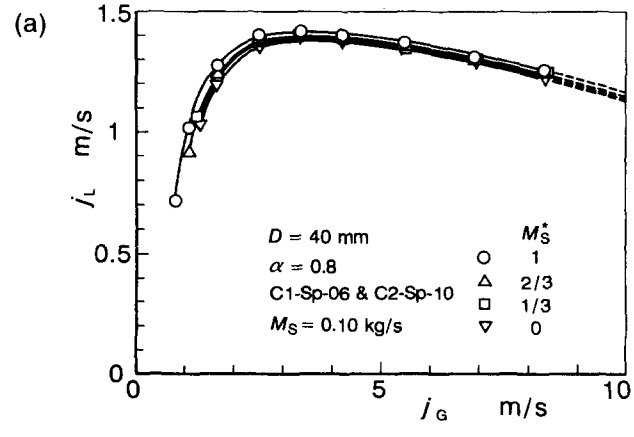

Figure 4(a). *Caption on p. 228.*

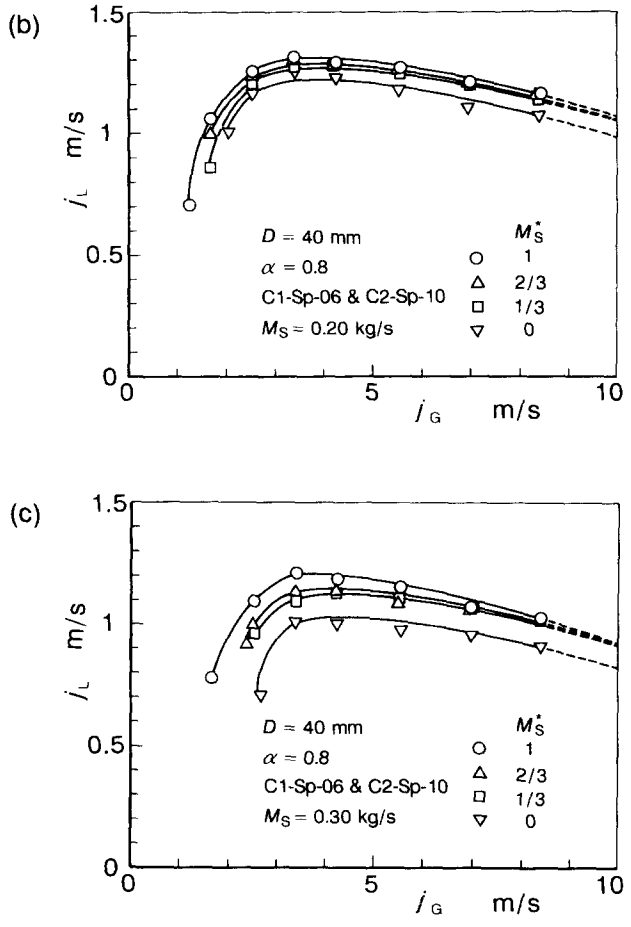

Figure 4. Relationships between the volumetric fluxes of air supplied and water discharged on an air-lift pump for conveying non-uniform particles: (a) $M_S = 0.10$ kg/s, (b) $M_S = 0.20$ kg/s and (c) $M_S = 0.30$ kg/s.

up of C1-Sp-06 and C2-Sp-10. This figure shows the relationship between j_G and j_L for given values of the mixing ratio, M_S^*. According to M_S^*, the experimental data are represented by each solid line. In each figure, with increasing M_S^*, j_L becomes high, i.e. the larger the flow rate of C1-Sp-06 becomes, the higher the j_L that results. Such a tendency is noticeable at a larger M_S, as seen in figure 4(c). As for other experimental results for the combination of C1-Sp-06 and C1-Sp-10, the data show trends similar to those of the above data concerning the combination of C1-Sp-06 and C2-Sp-10.

4. PREDICTION OF THE OPERATION PERFORMANCE

4.1. Momentum equation for a pump

An air-lift pump with a vertical, straight upriser having uniform cross-sectional area is illustrated in figure 5 together with a diagram of the pressure distribution, P, in the flow direction, z. The body of the air-lift pump consists of two parts; a suction pipe in which a two-phase water–solid mixture flows and an upriser in which a three-phase air–water–solid mixture flows. The symbols E, I and O denote the cross sections of the suction pipe inlet, the air injector and the upriser outlet, respectively.

A momentum equation is applied to a control volume bounded by the pipe wall and the cross sections E and O. Since the solid particles to be conveyed are, in general, non-uniform in size and

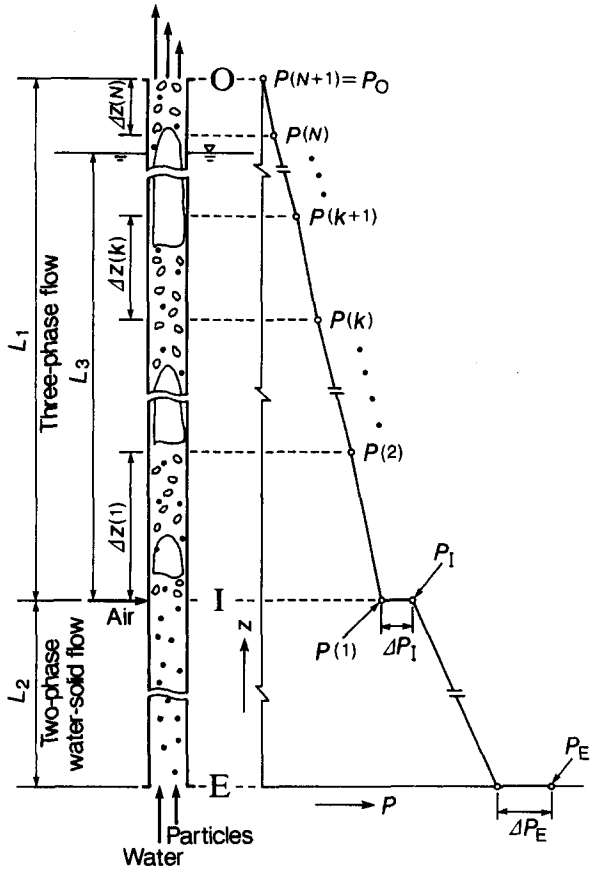

Figure 5. Diagram of a typical air-lift pump and the axial pressure distribution.

density, the particles are classified into n types according to size and density as shown in figure 6. The momentum equation may therefore be written as

$$
\begin{aligned}
&A\left\{j_{\mathrm{L}}\rho_{\mathrm{L}}u_{\mathrm{L,E}}+\sum_{i=1}^{n}j_{\mathrm{S}}(i)\rho_{\mathrm{S}}(i)u_{\mathrm{S,E}}(i)\right\}\\
&\quad-A\left\{j_{\mathrm{G,O}}\rho_{\mathrm{G,O}}u_{\mathrm{G,O}}+j_{\mathrm{L}}\rho_{\mathrm{L}}u_{\mathrm{L,O}}+\sum_{i=1}^{n}j_{\mathrm{S}}(i)\rho_{\mathrm{S}}(i)u_{\mathrm{S,O}}(i)\right\}\\
&\quad-\pi D\int_{\mathrm{E}}^{\mathrm{I}}\tau_{\mathrm{LS}}\,\mathrm{d}z-\pi D\int_{\mathrm{I}}^{\mathrm{O}}\tau_{3}\,\mathrm{d}z\\
&\quad-A\int_{\mathrm{E}}^{\mathrm{I}}\left\{\rho_{\mathrm{L}}\epsilon_{\mathrm{L,LS}}+\sum_{i=1}^{n}\rho_{\mathrm{S}}(i)\epsilon_{\mathrm{S,LS}}(i)\right\}g\,\mathrm{d}z\\
&\quad-A\int_{\mathrm{I}}^{\mathrm{O}}\left\{\rho_{\mathrm{G}}\epsilon_{\mathrm{G}}+\rho_{\mathrm{L}}\epsilon_{\mathrm{L,3}}+\sum_{i=1}^{n}\rho_{\mathrm{S}}(i)\epsilon_{\mathrm{S,3}}(i)\right\}g\,\mathrm{d}z\\
&\quad+A\{\rho_{\mathrm{L}}g(L_2+L_3)\}=0,
\end{aligned}
\qquad [2]
$$

where u is the velocity, ϵ the volumetric fraction, ρ the density, τ the shear stress, g the acceleration due to gravity and i the ith rank of the particles. The subscripts G, L, S, LS and 3 represent air, water, particles, the two-phase water–solid mixture and the three-phase air–water–solid mixture, respectively. The subscripts E, I and O represent the respective cross sections of the inlet, air injector and the outlet. In [2], the first and second terms denote the momentum which enters through E and leaves through O, the third and fourth terms denote the frictional pressure loss in the two-phase water–solid flow and in the three-phase flow, the fifth and sixth terms denote the weight of the

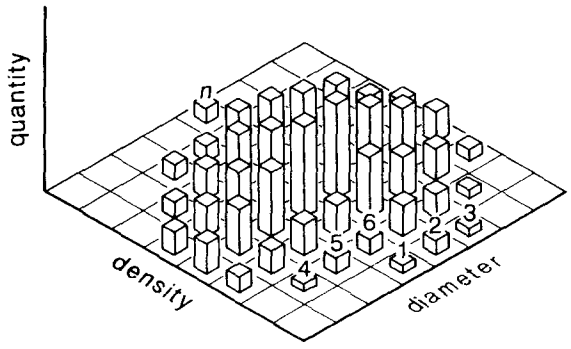

Figure 6. Classification of the particles according to their size and density.

two-phase water–solid mixture and of the three-phase mixture and the seventh term denotes the pressure force of the surrounding water acting on E.

To calculate the third–sixth terms on the left-hand side of [2], the axial pressure distribution is simplified. The pressure distribution is approximated stepwise as indicated by the bold line on the right-hand side of figure 5: the entrance pressure drop of the suction pipe, ΔP_E, which is the sum of the entrance fitting loss and the entrance length loss, occurs at E; the pressure drop in the suction pipe takes place from E to I; the entrance length loss of the upriser, ΔP_I, occurs at I; the pressure drop in the upriser takes place from I to O; the pressure at O is assumed to be equal to atmospheric pressure. The third and fifth terms on the left-hand side of [2] are, as a result, rewritten as

$$\pi D \int_E^I \tau_{LS}\, dz = A\left\{\frac{\Delta P_{f,LS}}{\Delta z} L_2 + \Delta P_E\right\} \qquad [3]$$

and

$$A \int_E^I \left\{\rho_L \epsilon_{L,LS} + \sum_{i=1}^{n} \rho_S(i)\epsilon_{S,LS}(i)\right\} g\, dz = A\left\{\rho_L \epsilon_{L,LS} + \sum_{i=1}^{n} \rho_S(i)\epsilon_{S,LS}(i)\right\} g L_2, \qquad [4]$$

where $\Delta P_{f,LS}/\Delta z$ in [3] is the frictional pressure gradient in the two-phase water–solid flow.

Since the frictional pressure gradient in the three-phase flow cannot be estimated at the middle of I and O due to the expansion of air, the upriser is divided into N nodes in the flow direction as shown in figure 5 following Weber & Dedegil (1976). Let $P(k)$ and $P(k+1)$ be the absolute pressures of the inlet and the outlet at the kth node. It is reasonable to equalize the values of $P(k)/P(k+1)$ for every node following Ueki (1977). Assuming that the pressure distribution of each node is linear, and the frictional pressure gradient of each node is calculated at the middle of each node. The fourth term on the left-hand side of [2] is, as a result, rewritten as

$$\pi D \int_I^O \tau_3\, dz = A\left\{\sum_{k=1}^{N} \frac{\Delta P_{f,3}(k)}{\Delta z(k)} \Delta z(k) + \Delta P_I\right\}, \qquad [5]$$

where $\Delta P_{f,3}(k)/\Delta z(k)$ is the frictional pressure gradient in the three-phase flow at the kth node.

Next, the gravity force of the three-phase mixture is estimated in the same way as the frictional pressure gradient: the gravity force at each node is estimated at the middle of each node. The sixth term on the left-hand side of [2] becomes

$$A \int_I^O \left\{\rho_G \epsilon_G + \rho_L \epsilon_{L,3} + \sum_{i=1}^{n} \rho_S(i)\epsilon_{S,3}(i)\right\} g\, dz = A \sum_{k=1}^{N} \left[\left\{\rho_G(k)\epsilon_G(k) + \rho_L \epsilon_{L,3}(k) + \sum_{i=1}^{n} \rho_S(i)\epsilon_{S,3}(k,i)\right\} g \Delta z(k)\right]. \qquad [6]$$

4.2. Correlations of volumetric fractions and pressure drops

ϵ_S, ϵ_G, ϵ_L, $\Delta P_{f,LS}/\Delta z$, $\Delta P_{f,3}/\Delta z$, ΔP_E and ΔP_I in [2]–[6] are obtained from the following correlations.

Volumetric fraction of particles. The volumetric fraction of particles belonging to the ith rank in a three-phase flow is expressed by

$$\epsilon_{S,3}(i) = \frac{j_S(i)}{u_S(i)}, \tag{7}$$

where $u_S(i)$ is the velocity of particles belonging to the ith rank in a three-phase flow.

According to correlations for the velocity of particles in a three-phase flow proposed by Sato *et al.* (1991), $u_S(i)$ is expressed by

$$u_S(i) = c\frac{m}{\rho_A} + u_{SW}(i), \tag{8}$$

where c is the distribution coefficient, m the mass flux of the three-phase mixture, ρ_A the apparent density of the three-phase mixture and $u_{SW}(i)$ the wall-affected settling velocity of the particles in an imaginary still three-phase mixture with ρ_A. c, m, ρ_A and $u_{SW}(i)$ are given as;

$$c = 1 + c_1 \exp\left\{-5\frac{\sum_{i_1=1}^{n}\epsilon_{S,3}(i_1)}{1-\epsilon_G}\right\}, \tag{9}$$

$$m = \rho_G j_G + \rho_L j_L + \sum_{i_1=1}^{n}\rho_S(i_1)j_S(i_1), \tag{10}$$

$$\rho_A = \left(\frac{\rho_3}{\rho_{LS,3}}\right)^{1.5}\rho_{LS,3}, \tag{11}$$

and

$$u_{SW}(i) = \left[1 - \left\{\frac{d_S(i)}{D}\right\}^2\right]\left\{1 - \frac{\sum_{i_1=1}^{n}\epsilon_{S,3}(i_1)}{1-\epsilon_G}\right\}^{2.4}\sqrt{\frac{\frac{\rho_L}{\rho_A}S(i)-1}{S(i)-1}}\,u_{ST}(i). \tag{12}$$

The factor c_1 in [9] is about 0.2 for a spherical particle. Sato *et al.* (1991) have proposed [11] by regarding a three-phase flow as a two-phase air–slurry flow. In [11], ρ_3 is the mean density of the three-phase mixture and $\rho_{LS,3}$ is the mean density of the slurry. These are expressed by

$$\rho_3 = \rho_G\epsilon_G + \rho_L\epsilon_{L,3} + \sum_{i_1=1}^{n}\rho_S(i_1)\epsilon_{S,3}(i_1), \tag{13}$$

and

$$\rho_{LS,3} = \rho_L\frac{\epsilon_{L,3}}{1-\epsilon_G} + \sum_{i_1=1}^{n}\rho_S(i_1)\frac{\epsilon_{S,3}(i_1)}{1-\epsilon_G}. \tag{14}$$

In [12], $S(i)$ is the specific density of the particle and $u_{ST}(i)$ is the free settling velocity of the single particle in still water. The exponent 2.4, which appeared in [12], is quoted from Richardson & Zaki (1954).

The volumetric fraction of particles in the two-phase water–solid flow, from the cross section E to I, is calculated from [7] by setting j_G and/or ϵ_G in [9], [10] and [12]–[14] equal to zero.

Volumetric fractions of the air and the water. Sato *et al.* (1991) proposed a correlation for the volumetric fraction of air in a three-phase flow. Their correlation is a modification of Smith's equation (1969–1970), which correlates the volumetric fraction of air in a two-phase air–water flow, with the flow rate of each phase regarding a three-phase flow as a two-phase air–slurry flow. The modified Smith's equation is

$$\epsilon_G = \left[1 + 0.4\frac{\rho_G}{\rho_{LS,3}}\left(\frac{1}{x}-1\right) + 0.6\frac{\rho_G}{\rho_{LS,3}}\left(\frac{1}{x}-1\right)\left\{\frac{\frac{\rho_{LS,3}}{\rho_G} + 0.4\left(\frac{1}{x}-1\right)}{1+0.4\left(\frac{1}{x}-1\right)}\right\}^{0.5}\right]^{-1}, \tag{15}$$

where the quality is given by $x = \rho_G j_G/m$.

If ϵ_S and ϵ_G are obtained, the volumetric fraction of water is automatically given by

$$\epsilon_{L,3} = 1 - \epsilon_G - \sum_{i=1}^{n} \epsilon_{S,3}(i). \quad [16]$$

Frictional pressure drop in the two-phase water–solid flow. $\Delta P_{f,LS}/\Delta z$ in [3] is calculated from the correlation proposed by Sadatomi *et al.* (1990a). Their correlation is a modification of Durand's equation (1953), which correlates the frictional pressure drop in two-phase liquid–solid flow replacing the liquid density with ρ_{LS}. The modified correlation is

$$\frac{\Delta P_{f,LS}}{\Delta z} = \lambda_{LS} \frac{1}{D} \frac{\rho_{LS}}{2} \left\{ j_L + \sum_{i=1}^{n} j_S(i) \right\}^2, \quad [17]$$

where the friction factor is given by

$$\lambda_{LS} = 0.316\, \mathrm{Re}_{LS}^{-0.25}. \quad [18]$$

The Reynolds number is expressed by

$$\mathrm{Re}_{LS} = \frac{\left\{ j_L + \sum_{i=1}^{n} j_S(i) \right\} D}{\nu_L}. \quad [19]$$

The validity of [17]–[19] has been confirmed by the experimental data for $D = 26$ mm, $d_S = 6$ mm, $\rho_S = 2540$ kg/m^3, $0.5 \leqslant j_L \leqslant 1.5$ m/s and $0.0075 \leqslant j_S \leqslant 0.060$ m/s, by Sadatomi *et al.* (1990a).

Frictional pressure drop in the three-phase flow. $\Delta P_{f,3}(k)/\Delta z(k)$ in [5] is calculated from the correlation proposed by Sadatomi *et al.* (1990b). Their correlation is similar to Chisholm & Laird's equation (1958), which correlates the frictional pressure drop in two-phase air–water flow: by regarding a three-phase flow as a two-phase air–slurry flow, Chisholm & Laird's equation is modified as

$$\varphi_{LS}^2 = \left\{ \frac{\Delta P_{f,3}(k)}{\Delta z(k)} \right\} \Big/ \left(\frac{\Delta P_{f,LS}}{\Delta z} \right) = 1 + \frac{21}{\chi} + \frac{1}{\chi^2}, \quad [20]$$

where

$$\chi^2 = \left(\frac{\Delta P_{f,LS}}{\Delta z} \right) \Big/ \left(\frac{\Delta P_{f,G}}{\Delta z} \right), \quad [21]$$

$$\frac{\Delta P_{f,G}}{\Delta z} = \lambda_G \frac{1}{D} \frac{\rho_G j_G^2}{2}, \quad [22]$$

$$\lambda_G = 0.316\, \mathrm{Re}_G^{-0.25} \quad [23]$$

and

$$\mathrm{Re}_G = \frac{j_G D}{\nu_G}. \quad [24]$$

The validity of [20]–[24] has been confirmed by the experimental data for $D = 26$ mm, $d_S = 6$ mm, $\rho_S = 2540$ kg/m^3, $0.5 \leqslant j_G \leqslant 8.0$ m/s, $0.5 \leqslant j_L \leqslant 1.2$ m/s and $0.0075 \leqslant j_S \leqslant 0.060$ m/s, by Sadatomi *et al.* (1990b).

Entrance pressure drop in the two-phase water–solid flow. ΔP_E in [3] is calculated from Dedegil's equation (1987) which correlates the entrance pressure drop in a suspension flow containing fine particles. By regarding the suspension as a two-phase water–coarse particles mixture, the equation can be written as follows:

$$\Delta P_E = (\xi + \zeta_E) \frac{\rho_{LS}}{2} \left\{ j_L + \sum_{i=1}^{n} j_S(i) \right\}^2, \quad [25]$$

where the coefficient of the inlet fitting loss, ξ, was set equal to 0.56, similar to the coefficient of the inlet fitting loss in a single-phase flow by Weisbach (1896), and the coefficient of the entrance length loss, ζ_E, was set equal to 1.0 following Dedegil (1987).

Entrance length loss in the three-phase flow. Similar to the entrance length loss of a single-phase flow, an additional pressure drop would occur at the cross section I because the kinematic energy of the two-phase water–solid mixture increases by injecting air. $\Delta P_{f,3}/\Delta z$ in [5] may therefore be written as

$$\Delta P_I = \zeta_I \left[\frac{\rho_{LS,3}}{2} \left\{ \frac{j_L + \sum_{i=1}^{n} j_S(i)}{1 - \epsilon_{G,I}} \right\}^2 - \frac{\rho_{LS}}{2} \left\{ j_L + \sum_{i=1}^{n} j_S(i) \right\}^2 \right]. \quad [26]$$

This correlation expresses the difference in the kinematic energy of the slurry upstream and downstream of the air injection. In [26], the kinematic energy of the air is neglected. The coefficient, ζ_I, was set equal to 1.0 in the present calculation.

4.3. Calculation procedure

For prescribed values of D, L_1, L_2, α, d_S, ρ_S, u_{ST} and N, if j_G and j_S are assigned, j_L can be calculated numerically from [2] by the iteration method. The step by step procedure is as follows:

(1) Select D, L_1, L_2, α, d_S, ρ_S, u_{ST} and N.
(2) Assign j_G and j_S.
(3) Determine $\Delta z(k)$ in the following manner assuming, as a first step, that the axial pressure distribution from I to O is linear; let $P(1)$ equalize the pressure on the outside of the pipe; calculate $P(k)/P(k+1)$ and $\Delta z(k)$.
(4) Compute j_G at I, O and the mid section of each node.
(5) Assume a value of j_L.

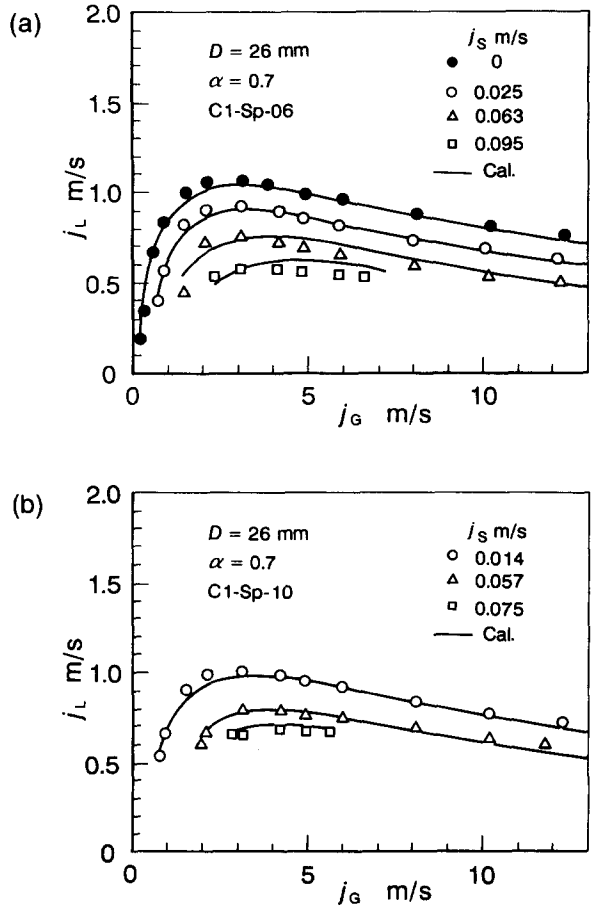

Figure 7(a, b). *Caption on p. 234.*

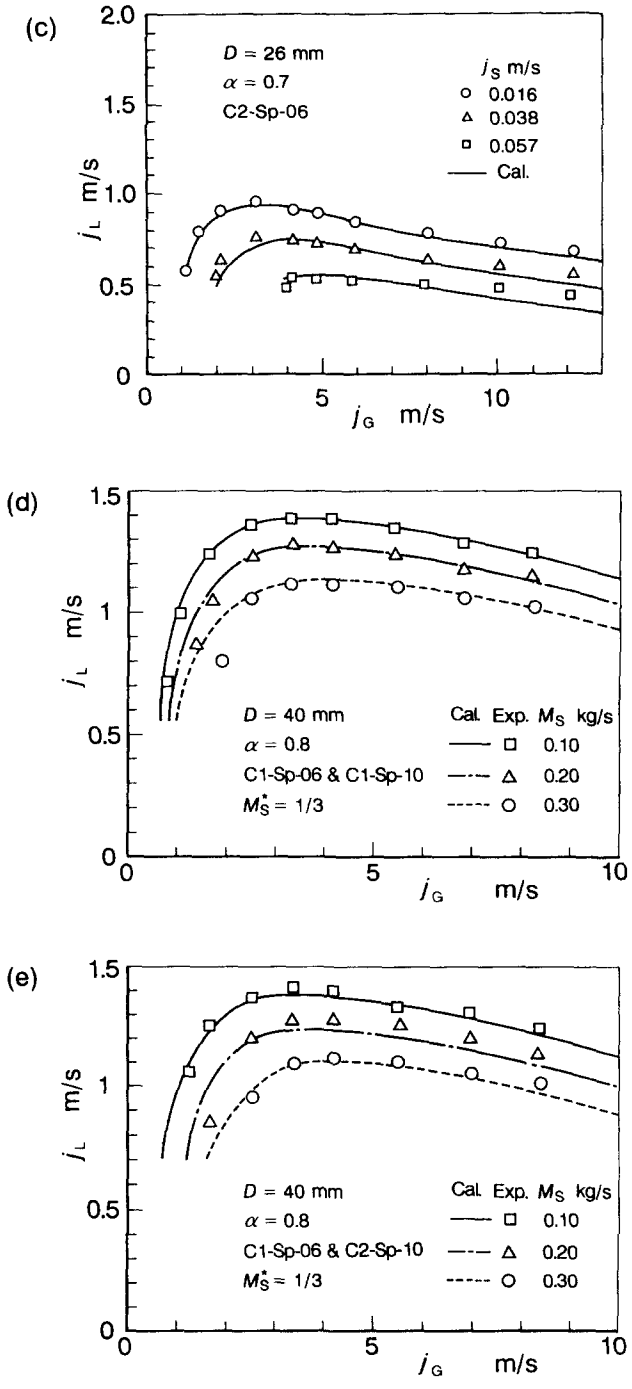

Figure 7.(a)–(c) Comparisons of the volumetric flux of water calculated by the present method with the present data; $D = 26$ mm, $\alpha = 0.7$ and uniform particles. (d) and (e) Comparisons of the volumetric flux of water calculated by the present method with the present data; $D = 40$ mm, $\alpha = 0.8$ and non-uniform particles.

(6) Calculate ϵ_G, ϵ_L and ϵ_S at I, O and the mid section of each node, and in the two-phase water–solid flow region from [7]–[16] by the bisection method.
(7) Calculate $\Delta P_{f,LS}/\Delta z$, $\Delta P_{f,3}(k)/\Delta z(k)$, ΔP_E and ΔP_I from [17]–[19], [20]–[24], [25] and [26], respectively.
(8) Calculate the value of the left-hand side of [2].

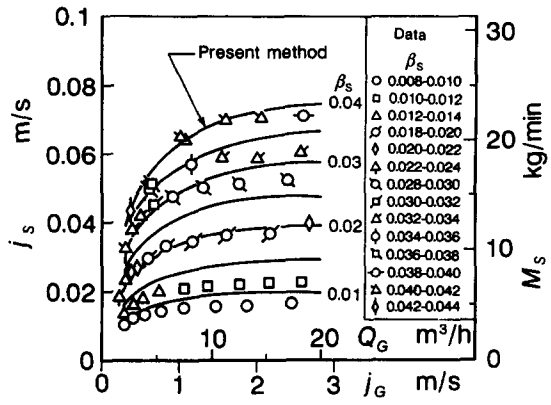

Figure 8. Comparisons of the volumetric flux of particles calculated by the present method with the experimental data of Kawashima *et al.* (1975); $D = 50$ mm, $L_1 = 6$ m, $L_2 = 0$, $\alpha = 0.92$, $d_S = 1.73$ mm, $\rho_S = 2670$ kg/m³ and $C_D = 2.44$.

(9) Repeat steps (5)–(8) until the total value on the left-hand side of [2] becomes nearly equal to zero.
(10) Renew $P(k)$.
(11) Repeat steps (4)–(10) until the new value of $P(1)$ becomes nearly equal to the old one, and output j_L.

The minimum number of N was examined with the experimental data of Weber & Dedegil (1976) which will be shown later in figure 10. As a result, we recommend selection of a suitable value of N as $P(k)/P(k+1)$ becomes less than 2.

In the analysis of the experimental data of other investigators, the pressure drop due to each singularity at E, I and O should be estimated as precisely as possible. However, it is also true that, unless an air-lift pump is extraordinarily short, the pressure drops due to singularities are small in comparison to those due to gravitation and friction. As a result, we have estimated the singularity pressure drops by means of the present respective correlations and coefficients if there is no description about the geometry of singularities.

5. DISCUSSION

5.1. Comparisons between the predictions and several investigators' experiments

Figures 7–10 show comparisons of j_L or j_S predicted by the present method with those obtained experimentally: figure 7(a)–(e) is concerned with the present experiments, whereas figures 8–10 are related to the experimental results of other investigators (Kawashima *et al.* 1975; Usami & Saito 1986; Weber & Dedegil 1976).

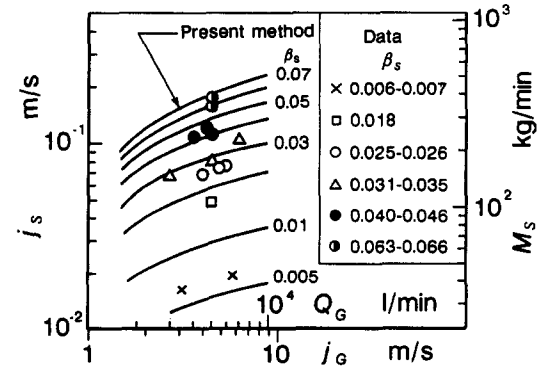

Figure 9. Comparisons of the volumetric flux of particles calculated by the present method with the experimental data of Usami & Saito (1986); $D = 155.4$ mm, $L_1 = 32.6$ m, $L_2 = 5.0$ m, $\alpha = 0.82$, $d_S = 36.3$ mm, $\rho_S = 1960$ kg/m³ and $C_D = 1.03$.

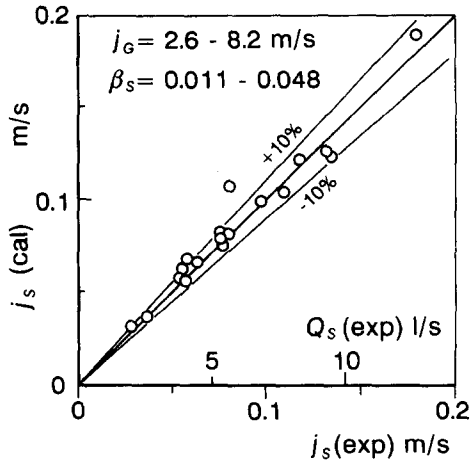

Figure 10. Comparisons of the volumetric flux of particles calculated by the present method with the experimental data of Weber & Dedegil (1976); $D = 300$ mm, $L_1 = 49.2$–253 m, $L_2 = 6.2$–351 m, $\alpha = 0.854$–0.973, $d_S = 5$ mm and $\rho_S = 2575$ kg/m^3.

Figure 7(a)–(c) is the result obtained from uniform particles, whereas figure 7(d) and (e) is from non-uniform particles for $M_S^* = 1/3$. Each predicted curve in figure 7(a)–(e) shows good fit to the experimental results except for the low range of j_G. It appears that the discrepancy between the present calculations and the experimental results at low j_G is mainly caused by the accuracy of the particle velocity; since the particle velocity becomes low at low j_G, the calculated values of ϵ_S would tend to be overestimated.

Figure 8 shows comparisons between the experimental results of Kawashima *et al.* (1975) and the present calculations. The presentation of the experimental results is the same as their original paper. They performed an experiment on an air-lift pump which conveyed gravel. Comparing their experimental conditions with those of the present experiments, their test particles were non-spherical and comparatively small in size ($d_S = 1.73$ mm), and j_G was low ($j_G < 3$ m/s). The calculations shown by solid lines give a fair representation of the experimental data.

Figure 9 is related to the experimental results of Usami & Saito (1986). The presentation of the experimental results is the same as their original paper. They performed an experiment on an air-lift pump with a slightly reclined upriser (5°), which conveyed simulated manganese nodules. In the present calculation, the upriser was assumed to be vertical (90°). The present calculations, shown by solid lines, on the whole agree with the experimental data.

Figure 10 shows comparisons of the experimental results of Weber & Dedegil (1976) with the present calculations. They performed an experiment on a large and tall air-lift pump which conveyed gravel. Their experimental conditions, L_1, L_2, α and β_S, were different from experiment to experiment. In the present calculation, the friction factor in the upriser was given as $\lambda = 0.0175$ per their suggestion. The present calculations are seen to be in good agreement with the experimental results within a margin of $\pm 10\%$.

At very high air flow rates, $j_G > 10$ m/s for example, it was difficult to confirm the validity of the present prediction method due to lack of data.

5.2. Comparisons between predictions of several investigators and the present experiment

Figure 11 shows comparisons of j_L predicted by other investigators' methods (Kawashima *et al.* 1975; Usami & Saito 1986; Dedegil 1987) with j_L obtained from the present experiment. The solid line shows the values calculated by the present method.

The method of Kawashima *et al.* (1975) shown in figure 11 uses a correlation about the volumetric fraction of air which has to be changed according to the flow pattern for the three-phase flow. Since the flow pattern for the present experiment in figure 11 is slug and churn flow, the calculation is shown by two convex curves. The calculation is not especially good at the boundary between the two flow patterns.

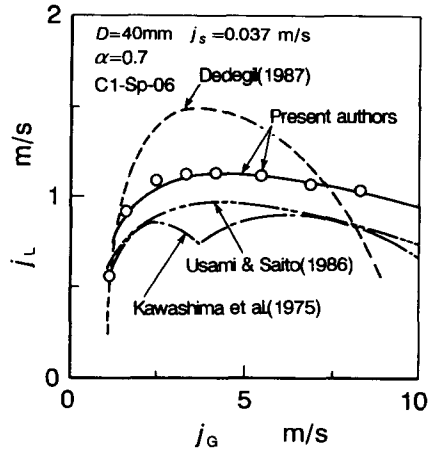

Figure 11. Comparisons of the volumetric flux of water calculated by four methods with the present experimental data; $D = 40$ mm, $\alpha = 0.7$, $d_S = 6.1$ mm, $\rho_S = 2540$ kg/m^3 and $j_S = 0.037$ m/s.

The method of Usami & Saito (1986) given in figure 11 employs the basic momentum equation. The calculation is qualitatively in good agreement with the experimental data but not quantitatively. The major factors which are responsible for the discrepancy between the calculation and the experiment are the coefficient of pressure losses other than frictional pressure loss and ϵ_G; the former was set to be equal to 3.5 by inference from their paper, the latter was 5–15% lower than ϵ_G calculated by the present method.

The power balance equation of Dedegil (1987) is also shown in figure 11. The agreement between the calculation and the experiment is not so good. The discrepancy is attributable to the estimation of air volume fraction and frictional pressure loss; the calculation becomes larger than the experimental results because ϵ_G was larger by about 10% than that predicted by the present method at $j_G > 2$ m/s, and the calculation becomes lower than the experimental results because the frictional pressure loss was about twice as much as the present method at $j_G > 4$ m/s.

None of the methods proposed by other investigators show particularly good fits to the present experimental results. It seems that the discrepancy is attributable to the range of application, i.e. those investigators have derived their methods based on their experiment and verified the applicability by their own experimental data alone.

6. SUMMARY AND CONCLUSIONS

(1) We performed experiments on an air-lift pump for conveying coarse particles by systematically changing the diameter of the pipe, the diameter of the spherical particles and the submergence ratio, and we obtained experimental data which represent the triangular relationship between the flow rate of air supplied and the flow rates of water and particles discharged.

(2) We explained the operation performance of an air-lift pump with an explanatory curved surface which was drawn from the triangular relationship.

(3) We proposed a prediction method for operation performance of an air-lift pump which conveys non-uniform particles. The validity of the method was confirmed with the experimental results of the present authors and three other investigators. It was seen, as a result, that the present method was valid not only for the relatively small-scale air-lift pumps installed in a laboratory but for relatively large and tall ones of 300 mm in diameter and 250 m in length.

Acknowledgements—The authors wish to express their gratitude to Dr Sadatomi, Kumamoto University, for stimulating discussion on this work and to the graduate students at Nishinippon Institute of Technology for their help in performing the experiments.

REFERENCES

Chisholm, D. & Laird, A. D. K. 1958 Two-phase flow in rough tubes. *Trans. ASME* **80**, 276–286.

Dedegil, M. Y. 1987 Principles of air-lift techniques. In *Encyclopedia of Fluid Mechanics* (Edited by Chereimisinoff, N. P.), Vol. 4, Chap. 12., Gulf, Houston, TX.

Durand, M. R. 1953 Ecoulements de mixture en conduites verticales—influence de la densite des materiaux sur les caracteristiques de refoulement en conduite horizonatale. *La Houille Blanche* **8**, 124–130.

Giot, M. 1982 Three-phase flow, In *Handbook of Multiphase Systems* (Edited by Hetsroni, G.), para. 7.2.. McGraw–Hill, New York.

Kato H., Miyazawa, T., Timaya, S. & Iwasaki, T. 1975 A study of an air-lift pump for solid particles. *Bull. JSME* **18**, 286–294.

Kawashima, T., Noda, K., Masuyama, T. & Oda, S. 1975 Hydraulic transport of solids by air lift pump. *J. Mining Metall. Inst. Japan* **91**, 765–772. In Japanese.

Richardson, J. F. & Zaki, W. N. 1954 Sedimentation and fluidisation—part 1. *Trans. Inst. Chem. Engrs* **32**, 35–53.

Sadatomi, M., Sato, Y., Yoshinaga, T. & Inagaki, K. 1990a Hydraulic lifting of coarse particles in vertical pipes—1st report, liquid–solid two-phase flow. *Jap. J. Multiphase Flow* **4**, 111–124. In Japanese.

Sadatomi, M., Sato, Y., Yoshinaga, T. & Maeda, S. 1990b Hydraulic lifting of coarse particles in vertical pipes—2nd report, gas–liquid–solid three-phase flow. *Jap. J. Multiphase Flow* **4**, 125–140. In Japanese.

Sato, Y., Yoshinaga, T. & Sadatomi, M. 1991 Data and empirical correlation for the mean velocity of coarse particles in a vertical three-phase air–water–solid particle flow. *Proc. Int. Conf. Multiphase Flow '91—Tsukuba*, Vol. 1, Tsukuba, Japan, pp. 363–366.

Smith, S. L. 1969–1970 Void fractions in two-phase flow: a correlation based upon an equal velocity head model. *Proc. Inst. Mech. Engs* **184**, 647–664.

Tomiyama, A., Furutani, N., Minagawa, H. & Sakaguchi, T. 1992 Numerical analyses of air lift pumps based on the multi-fluid model. *Jap. J. Multiphase Flow* **6**, 173–188.

Ueki, S. 1977 Studies on air lift (Part 2). *Mining Safety* **25**, 393–405. In Japanese.

Usami, T. & Saito, T. 1986 Studies on the hydraulic lifting of solids by air-lift pump. Report of the National Research Institute for Pollution and Resources 38, pp. 1–101. In Japanese.

Weber, M. & Dedegil, M. Y. 1976 Transport of solids according to the air-lift principle. *Proc. 4th International Conf. on the Hydraulic Transport of Solids in Pipes*, Alberta, Canada, pp. H1–1-23 and X93-94.

Weisbach, J. 1896 *Ingenieur und Maschienen Mechanik*, Vol. 1, p. 1003.